ANTI-PHASE SIGNATURE OF FLARE GENERATED TRANSVERSE LOOP OSCILLATIONS

R. S. WHITE, E. VERWICHTE, AND C. FOULLON

Centre for Fusion, Space and Astrophysics, Department of Physics, University of Warwick, Coventry CV4 7AL, UK; r.s.white@warwick.ac.uk

ABSTRACT

Transverse loop oscillations observed by the Atmospheric Imaging Assembly instrument on the *Solar Dynamics Observatory* spacecraft are studied after an impulsive solar flare eruption on 2012 May 8. We have found that a transversely oscillating coronal loop seen in the 171 Å bandpass oscillates in anti-phase with respect to adjacent larger loops seen in the 193 Å and 211 Å bandpasses. These unusual oscillations are analyzed to investigate the excitation mechanism responsible for their initial inwardly directed anti-phase behavior. The transverse oscillations are analyzed by constructing space-time diagrams from cuts made parallel to the projected loop displacements. The displacement time oscillation profiles are background subtracted and fitted with a damped cosine curve that includes a linear change in the period with time. The local magnetic topology of the active region is modeled using potential field source surface extrapolation. It reveals that the loops are anchored in different topological regions with foot point locations identified on either side of the EUV flare peak emission source. In this context, the oscillation characteristics indicate that the excitation mechanism is closely linked to the local magnetic field topology and the reconnection generated wave dynamics in the active region rather than following an external flare blast wave. We discuss how observations such as these may serve to identify reconnection processes in similar quadrupolar active regions.

Key words: magnetohydrodynamics (MHD) – Sun: corona – Sun: flares – Sun: oscillations – Sun: UV radiation

Online-only material: color figures, animation

1. INTRODUCTION

The *Solar Dynamics Observatory* (*SDO*) era of observations has continued to shed light on a wide variety of magneto-hydrodynamic wave modes (Nakariakov & Verwichte 2005) by taking advantage of instruments such as the Atmospheric Imaging Assembly (AIA; Lemen et al. 2012; Boerner et al. 2011), which observes the corona in remarkable detail. Observations of coronal wave modes using a variety of instruments include global (EUV) waves (Ma et al. 2011; Muhr et al. 2011; Asai et al. 2012), kink Alfvénic waves (Nakariakov et al. 1999; Tomczyk et al. 2007; Verwichte et al. 2004; Aschwanden & Schrijver 2011; McIntosh et al. 2011; Hershaw et al. 2011; White & Verwichte 2012; White et al. 2012; Gosain & Foullon 2012; Nisticò et al. 2013), and slow waves (De Moortel et al. 2000; Wang et al. 2003; Kiddie et al. 2012; Krishna Prasad et al. 2012a, 2012b). Each of these wave modes reveals something about the structure of the corona through which they travel and can be utilized as seismological tools to determine parameters such as the magnetic field strength (Nakariakov & Ofman 2001) or to investigate processes such as the dissipation of energy leading to heating (Roberts 2000). Transverse loop oscillations (TLOs) in particular can be used as a diagnostic tool for the coronal magnetic field strength through the relation between the kink speed and the phase speed. Magnetic field estimates can be improved by including density diagnostics from spectroscopy instruments, e.g., Van Doorsselaere et al. (2008), and observations of TLOs can be combined with magnetic extrapolation techniques to further probe local coronal plasma properties (Verwichte et al. 2013).

Traditionally it has been believed that TLOs are excited by an impulsive event such as a solar flare which can produce a blast wave, perturbing the surrounding corona (Aschwanden et al. 1999; Nakariakov et al. 1999; Hori et al. 2005; Van Doorsselaere et al. 2009; Verwichte et al. 2010; Tothova et al.

2011; Wang et al. 2012). However a TLO observed in a post flare hot (>10 MK) loop was proposed to have a different excitation mechanism where the reconnection processes are thought to play an important role in both the formation of the loop and the perturbation of the transverse oscillation (White et al. 2012). Impulsively excited TLOs are usually observed to have their initial displacement away from the source of excitation and then to damp rapidly back to an equilibrium which may or may not be aligned with their initial start position, e.g., White & Verwichte (2012).

Anti-phase transverse oscillations in coronal loops have been observed by Schrijver & Brown (2000). They observe transverse oscillations that occur after a flare with the *Transition Region and Coronal Explorer* (*TRACE*) spacecraft. To explain the anti-phase behavior of the oscillations they suggest that the magnetic topology of the active region plays an important role. They describe how a small shift of a null point will cause a field line passing close by to experience a considerable change in position, where the direction of motion of the field line will be affected by the direction of shift of the null point. In general the magnetic topology of active regions has not been of interest when discussing TLOs and their excitation; however, the local magnetic topology might also help to explain why some active region loops oscillate while other loops in the same active region do not (the so called "selectivity problem") even though they appear to be similar structures. Anti-phase oscillatory signatures have also been detected in Solar Ultraviolet Measurements of Emitted Radiation (SUMER) spectral data during a solar flare on the east solar limb (Kliem et al. 2002). They observe coronal material in hot lines (Fe XXI formed at $\sim 10^7$ K) and cool lines (C II formed at $\sim 2 \times 10^4$ K) that show anti-phase behavior in their Doppler line shifts. Like TLOs, these Doppler shift oscillations are observed to damp on short timescales, however they rule out TLOs as an explanation in this case because the anti-phase Doppler line shifts are observed at low coronal heights

with amplitudes that were three times larger than the largest TLO amplitudes detected by *TRACE* (Aschwanden et al. 2002). Large displacements associated with TLOs have since been reported by Verwichte et al. (2010). Alternative explanations in terms of impulsively generated propagating waves or relaxation oscillations of flows were proposed instead as the cause of the anti-phase oscillations observed in the different temperature lines.

In this paper we present an *SDO*/AIA observation of TLOs displaying anti-phase oscillations initially directed inward toward each other after an impulsive flare event. This is an unusual observation because from previous studies (e.g., Aschwanden et al. 2002; White & Verwichte 2012) we would expect the loops to begin oscillating in phase. We investigate the local magnetic topology of the active region to help explain the origin of these unusual oscillations and show that TLOs are a potential tool for identifying dynamic reconnection processes in active regions. Section 2 outlines the observation, Section 3 describes the analysis of the TLOs and in Section 4 magnetic field extrapolation using the potential field source surface (PFSS) model is performed. The results are discussed in Section 5.

2. OVERVIEW OF THE OBSERVATIONS

We study TLOs present in active region NOAA 11476 on 2012 May 8. The active region is situated on the NE solar disk and produced a number of flares over several hours including an M1.4 *GOES* class flare peaking at 13:08 UT in the soft X-ray channel. The flaring associated with the most energetic particles peaked at 13:07 UT (N13° E44°) as recorded in Hα ground-based observations (San Vito, Italy) and as measured in hard X-rays (25–50 keV) by *RHESSI*. The event is observed by *SDO*/AIA and is shown in six of the AIA channels (171 Å, 193 Å, 211 Å, 131 Å, 94 Å, and 304 Å) in Figure 1. Three images of the active region in each of the bandpasses are displayed before (12:50 UT) and after the flare peak (13:10 UT, 13:30 UT). An animation of the event combining the 171 Å (green), 211 Å (red), and 131 Å (blue) AIA bandpasses is available in the online journal. AIA's unique capabilities allow the event to be observed in a wide temperature range with a time cadence of 12 s and a pixel resolution of 0″.6. Loop structures are visible in all bandpasses and a band of hot emission in the vicinity of the loops in the 131 Å and 94 Å channels is observed. In addition this hot emission is seen in *Hinode* X-Ray Telescope (XRT) images both before and after the flare eruption. Fan-like structures are visible in multiple AIA channels on either side of the loop structures that exist before and after the eruption. The active region is also visible on the limb with the Extreme Ultraviolet Imager (EUVI) on the *Solar Terrestrial Relations Observatory* (*STEREO*) *B* spacecraft (Howard et al. 2008); however, individual loops observed by AIA are difficult to identify in the EUVI images. The field of view of the EUV imaging spectrometer on *Hinode* was just below the loop structures so spectral information of the loops is not available.

Figure 2 shows the active region before the flare peak in the 171 Å (left panel) and 131 Å (right panel) AIA bandpasses. Both images show fan (with respect to the field of view of the figure) and closed loop structures situated above a complex (Hale sunspot classification of $\beta\gamma/\beta\gamma$) magnetic field configuration shown by a magnetogram from the Helioseismic and Magnetic Imager (HMI) on *SDO* (middle panel). The flare is located at position (−660″ E, 260″ N) and during the eruption, flare ribbons create an inverted Y shape structure that is seen in the EUV images. The HMI magnetogram indicates that the flare
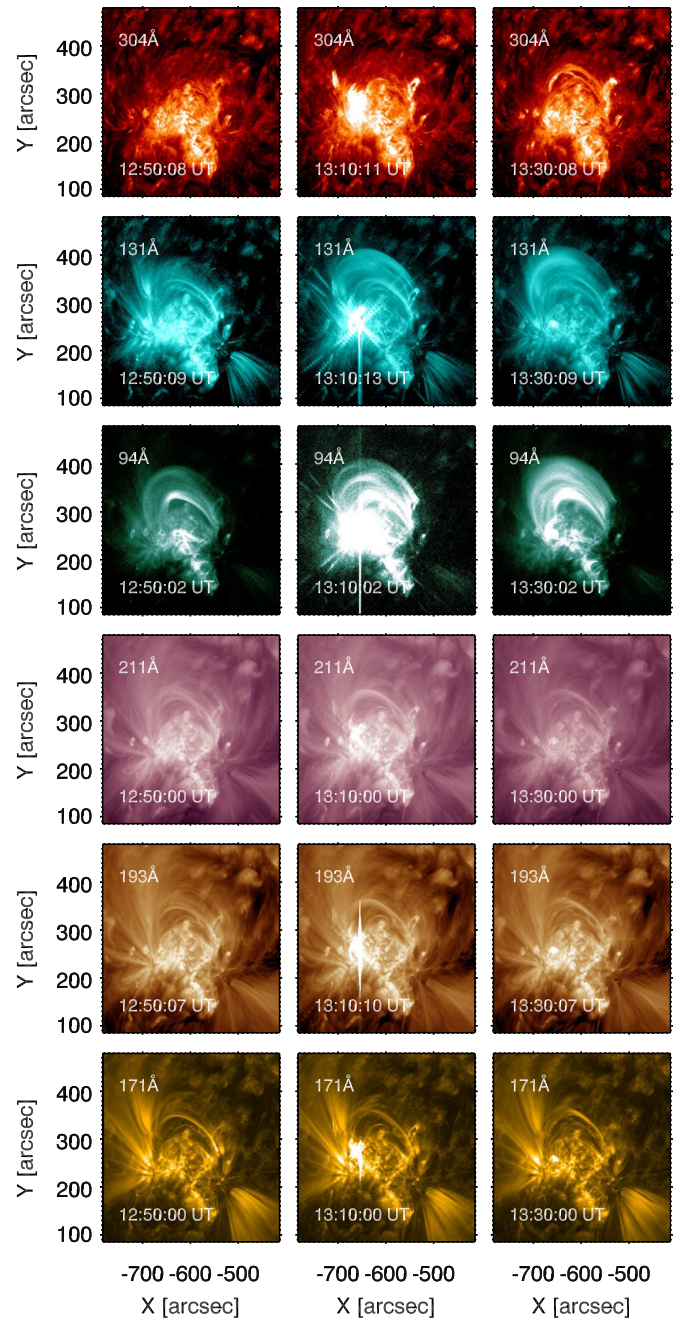

Figure 1. Active region 11476 on 2012 May 8 displayed in six extreme-ultraviolet *SDO*/AIA bandpasses for three different times covering the duration of the flare and transverse loop oscillations. Left: 12:50 UT, middle: 13:10 UT, and right: 13:30 UT. Transverse loop oscillations are reliably observed in the 171 Å, 193 Å, and 211 Å bandpasses.

(An animation and a color version of this figure are available in the online journal.)

ribbons are located on or close to polarity inversion lines, in a region where there is negative flux surrounded by positive flux.

The flare eruption excites several loops to oscillate with transverse motions, which we study in more detail. Paths showing the loop positions are shown in Figure 2. The lower loop indicated by the dashed line is observed particularly strongly in the 171 Å bandpass while the loop above this indicated by the solid and dotted lines is seen most clearly in the 193 Å and 211 Å channels, respectively. The loop paths indicate how much of the loop is visible in the images before the line of sight confusion renders it too difficult to identify individual loops.
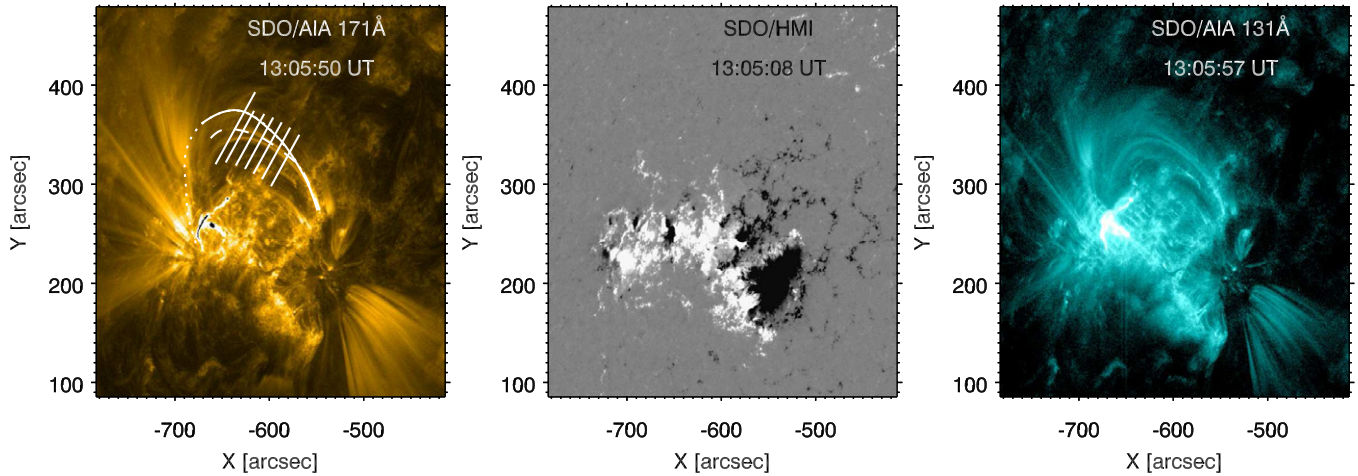
Figure 2. Left: 171 Å AIA image of the active region. The loops studied in three *SDO*/AIA bandpasses for their transverse oscillations are indicated by the curved lines: 171 Å (dashed line), 193 Å (solid line), and 211 Å (solid and dotted line). The straight solid lines are the cuts taken to analyze the transverse oscillations. Middle: *SDO*/HMI magnetogram showing the line-of-sight magnetic field at the photosphere. Right: 131 Å AIA image. The flare ribbons make an inverted Y shape.
(A color version of this figure is available in the online journal.)

The loops observed in 193 Å and 211 Å have overlapping loop paths and displacement time series positions. This suggests that they are likely to be the same loop structure that has multi-thermal components. The western loop foot points appear to be the same for each of the loops and originate in a region of negative polarity above the large sunspot region; however, the location of the eastern foot points are hidden by many other intense structures in the line of sight. From studying the data we expect the eastern foot points to lie close to the site of the EUV flare emission. The TLOs fit the typical characteristics of previously observed TLOs, i.e., an impulsive trigger and short damping timescales. During the flare, material visible in all AIA channels is ejected and observed to follow field line trajectories, flowing along and then back down toward the chromosphere. Interestingly the loop observed in the 193 Å and 211 Å channels displays impulsive oscillations that are initially directed south in the AIA field of view, whereas the loop in the 171 Å is pushed away from the southern source region as we would expect for an impulsive event. This inwardly directed anti-phase behavior is unusual and we investigate this intriguing observation further.

3. ANALYSIS

Analysis of the transverse oscillations is conducted using the method of taking space time cuts parallel to the projected loop displacement and fitting the background subtracted displacement time series with a damped cosine curve to obtain the oscillation parameters. See, e.g., White & Verwichte (2012) for further details on this method. The paths along which the cuts are taken to analyze the transverse oscillations are shown in the left panel of Figure 2. The angles of the paths are determined by a trial and error approach of identifying the clearest oscillations with the largest amplitudes. If an accurate estimate of the three-dimensional (3D) loop geometry is found (not available in this case) then the cuts can be precisely aligned with the projected loop displacement. Where possible, the displacement time series is determined automatically by fitting a Gaussian shape to the loop cross section at each time; however, in most cases the displacement time series is determined by eye.

Figure 3 shows wavelet filtered space-time diagrams for a single cut from the three AIA bandpasses, 171 Å, 193 Å, and 211 Å, where transverse oscillations are detected. The

displacement time series are indicated on each cut and the vertical dashed line at 13:06 UT indicates the reference time where the oscillations begin. A background polynomial of up to the order of four is subtracted from the displacement time series and a damped cosine profile is fitted using a Levenberg–Marquardt least-squares method (Markwardt 2009) to determine the oscillation parameters. Similar to the method used in Foullon et al. (2010) and Gosain & Foullon (2012) to analyze quasi-periodic pulsations in solar flares and transverse oscillations of prominences, respectively, we find that the displacement time series are almost always best fitted by a profile that includes a linear change in the period with time, e.g.,

$$\xi(t) = \xi_0 \exp\left(\frac{-(t - t_0)}{\tau}\right) \cos\left(\frac{2\pi}{P + \alpha\,(t - t_0)}\,(t - t_0) - \phi\right),$$
(1)

where ξ_0 is the displacement, τ is the damping time, P is the period, α is the rate of change in the period, ϕ is the phase, and t_0 is the reference time. The errors on the oscillation parameters are taken as the standard deviation of the results from several cuts. Table 1 shows the oscillation parameters determined from the damped cosine profile fitting for each of the loops in the three bandpasses. The phases found by the profile fitting technique (and shown by the displacement profiles in Figure 3) show that the 171 Å loop ($\phi = -28 \pm 3°$) is initially oscillating in anti-phase with respect to the loops analyzed in the 193 Å ($\phi = 135 \pm 14°$) and to a lesser extent the 211 Å ($\phi = 123 \pm 17°$) bandpasses. The 193 Å and 211 Å loop periods are comparable to one another whereas the period of the 171 Å loop is approximately 50 s longer. Figure 3 also shows that the 171 Å loop has a slightly longer period in this cut compared to the other loops; however, at a later time the displacement time profiles of each of the loops look to be in phase. The damping times show the characteristic short damping times expected for TLOs. Both the analysis and Figure 3 suggest that the loops observed by the 193 Å and 211 Å bandpasses are part of the same multi-thermal loop structure rather than two distinct loops. The linear change in the period determined from the damped cosine fitting was positive for each of the loops analyzed, suggesting that the period increases slightly during the oscillation. The example
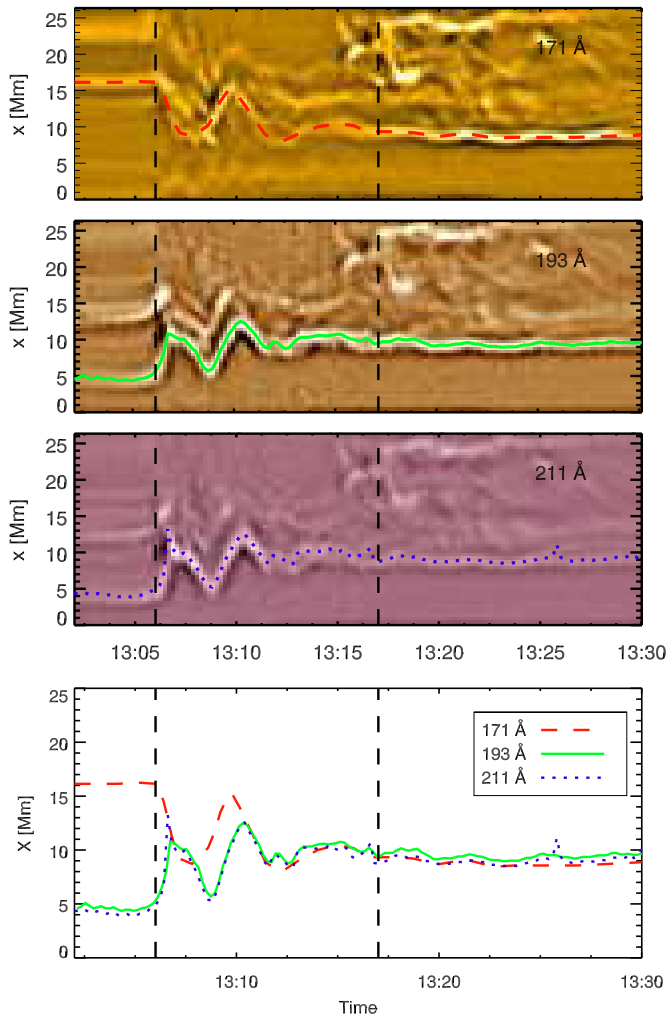
3

Figure 3. Example space-time images from a cut taken across the transversely oscillating loops are shown for the 171 Å, 193 Å, and 211 Å bandpasses. The images have been wavelet filtered using the Mexican hat wavelet. The anti-phase nature between the 171 Å loop and the loop observed in the 193 Å and 211 Å bandpasses is clearly visible and the displacement time series are indicated on the cuts. Bottom: the displacement time series are plotted on the same plot to highlight the anti-phase nature of the oscillations and to show how they compare spatially with one another. The reference times of 13:06 UT and 13:17 UT shown by the vertically dashed lines indicate the start of the initial high amplitude and later low amplitude oscillations respectively.

(A color version of this figure is available in the online journal.)

Table 1
Displacement Oscillation Parameters Determined
from the Damped Cosine Fitting

Loop	P (s)	τ (s)	ϕ (°)	α
		Displacement		
171	224 ± 30	267 ± 70	-28 ± 5	0.179 ± 0.100
193	174 ± 10	271 ± 40	135 ± 10	0.071 ± 0.020
211	180 ± 10	285 ± 80	123 ± 20	0.059 ± 0.030
171b	196 ± 10	1295 ± 720	149 ± 20	0.008 ± 0.010
193b	194 ± 10	582 ± 190	149 ± 10	0.015 ± 0.100[a]
		Intensity		
193	171 ± 20	378 ± 160	143 ± 30	0.069 ± 0.040
211	151 ± 20	404 ± 240	152 ± 30	0.088 ± 0.030
193b	198 ± 10	834 ± 150	108 ± 30	0.006 ± 0.010

Note. [a] Indicates the value is the result obtained for one cut only.

These oscillations are most likely a result of the plasma ejection from the flare site which flows along the field lines, perturbing them. Material ejected along field line trajectories to the south of the oscillating loops is visible in the top right part of the cuts. These lower amplitude oscillations are observed exclusively in the 171 Å and 193 Å bandpasses and show oscillations that are in phase with similar periods. Table 1 shows the results for these oscillations labeled 171b and 193b.

Any intensity oscillations present in the loops are investigated in the same way as for the displacement time series but taking the intensity located at each time series position. The intensity oscillations are also fitted with the damped cosine curve that includes a linear variation in the period. Results are shown in Table 1. Reliable intensity oscillations are observed for the 193 Å and 211 Å loops and the later, lower amplitude oscillation in the 193 Å bandpass. The intensity oscillations show approximately in phase behavior with the displacement time series for the 193 Å and 211 Å bandpasses.

4. ACTIVE REGION TOPOLOGY

4.1. 3D Loop Geometry

An estimate of the 3D loop geometry is found by comparing the loops in the AIA viewpoint with the loops observed on the limb by *STEREO-B*/EUVI in the 171 Å and 195 Å wavelengths. During this observation *STEREO-B* was approximately 118° behind the Earth viewpoint. See, e.g., Verwichte et al. (2009, 2010) for details of the procedure for obtaining a 3D loop geometry. As a result of the reduced resolution compared with AIA and the fact that the loops are observed on the limb in EUVI, identifying and distinguishing loops from one another to get an accurate geometry is challenging. Using this method an approximate inclination angle of 43° north and a loop length of 195 Mm is found. This length is likely to be an underestimate of the true length of the loops since the best fit to the EUVI data was found by following the bright loop structure seen in all of the AIA bandpasses in Figure 1, which is below the loops studied (traced by the lines in Figure 2). There is a possibility that the anti-phase oscillations are a result of line of sight effects rather than a true anti-phase motion of loops. This possibility occurs if the loops are of opposite inclination with respect to the plane of sky. The comparison of the loop geometry shows that these loops located on the northeast solar disk are highly inclined on the same side behind the plane of sky, suggesting
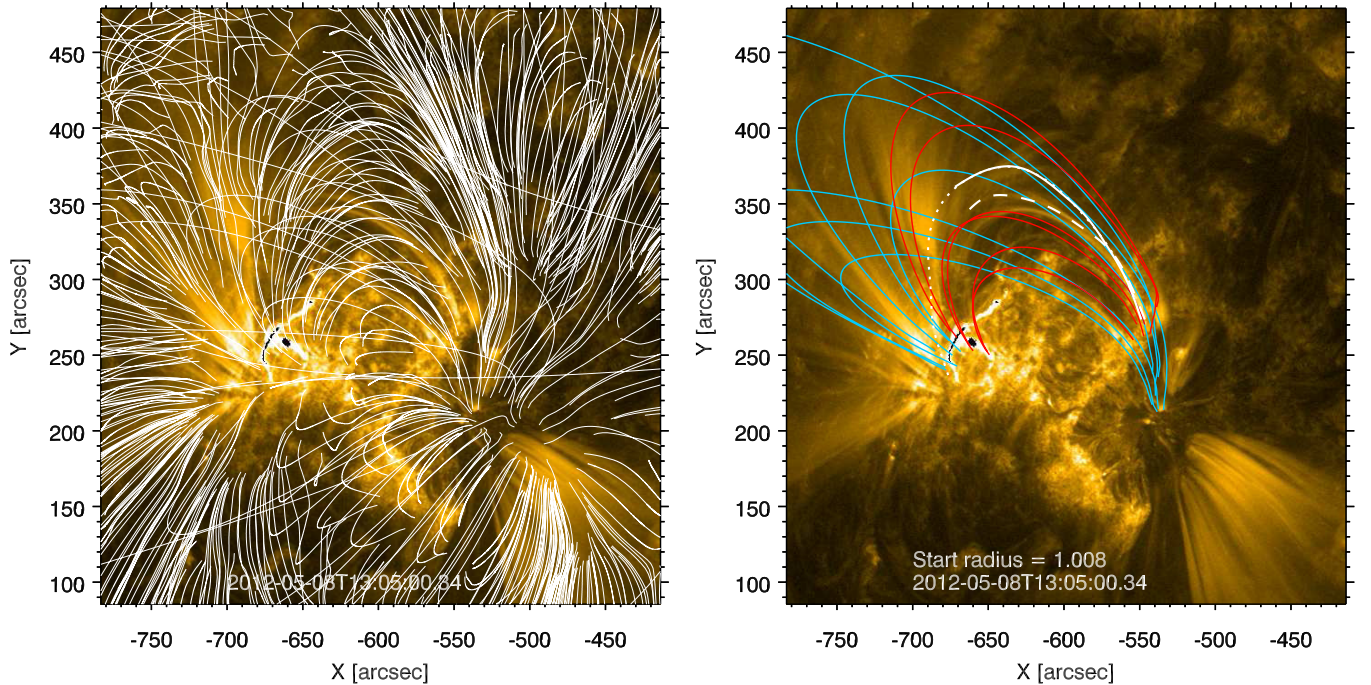
displacement time profiles from the three different wavelengths are compared in the bottom panel. This shows that the loops are perturbed at the same time with transverse oscillations that are initially directed inward toward each other. Loop structures observed in the 193 Å and 211 Å bandpasses visible at $x = 13$ Mm begin to move inward slightly before the hard X-ray flare peak (13:07 UT) and the excitation of the 171 Å loop highlighted by the dashed line. This early inward motion may indicate that the loops are not instantaneously excited but that the excitation has a finite time width over which it ramps up, causing the loops to move inward slightly earlier than the flare peak. At the end of the oscillations the loops that started at positions $x = 5$ Mm (193 Å and 211 Å) and $x = 16$ Mm (171 Å) have relaxed to the same position of $x = 9$ Mm.

Transverse oscillations are also excited at a later time in the same loops, beginning at approximately 13:17 UT (second vertical dashed line in Figure 3), but displaying smaller amplitudes.

Figure 4. Left: plotted on a 171Å *SDO*/AIA image are field lines calculated using the PFSS model with a starting radius of 1.008 solar radii. Right: bundles of field lines that have different foot point positions are plotted to search for topological differences. The loop paths traced in the EUV images are overlaid in white as a comparison with the extrapolated field lines.

(A color version of this figure is available in the online journal.)

that the anti-phase oscillations are not a result of line of sight effects.

4.2. Magnetic Field Topology: PFSS Modeling

To probe the magnetic topology of the active region, magnetic field extrapolation is performed using the PFSS model (Schatten et al. 1969; Schrijver 2001; Schrijver & De Rosa 2003). The extrapolation technique incorporates line-of-sight magnetogram data from *SDO*/HMI near the central meridian and extrapolates the magnetic field out to a distance of 2.5 solar radii where it is then assumed radial. The most up to date magnetic map for a particular region of interest is obtained when the region has crossed the central meridian. In this observation the active region is located near N13° E44° on May 8 and has completely crossed the central meridian by May 13. Therefore, in our analysis we use the coronal magnetic field model for data up to 2012 May 13, five days after the flare eruption.

The left hand panel of Figure 4 shows the extrapolated field lines overlaid on an AIA 171 Å image. We are interested to see if there are any differences between individual field lines such as the location of the foot points that may indicate different topological regions and give rise to the anti-phase oscillations. No particular topological differences between field lines are immediately apparent from overlaying the extrapolated field on the AIA image. To investigate this further, field lines with foot points that are anchored in different positions on the eastern and western sides are plotted in different colors. This is shown in the right hand panel of Figure 4. The loop paths of the AIA observed loops are also drawn on this plot. On the western side the red field lines are anchored in the negative flux region above the blue field lines, which are anchored in the large negative sunspot. The observed 171 Å loop path shown by the dashed white line is seen to follow closely to a couple of the red field lines. On the east side of the active region the field lines are anchored at the same

position as the flare ribbons. The blue field lines are located on the opposite side of the negative flux from some of the smaller red field lines. Both sets of eastern foot points must be located in regions of positive flux as their western foot points are anchored in negative flux regions. Figure 5 shows a negative polarity at $X = -660''$, $Y = 250''$ that has disappeared by May 13.

The loop paths in the 193 Å and 211 Å channels (shown by the solid and dotted white lines) have larger radii of curvature and are therefore expected to have larger apex heights and foot point distances than the 171 Å loop. Since the active region is evolving over the following days with the eruption of five M class and several C and B class flares, it is not surprising that their paths do not perfectly align with any of the PFSS field lines, which represent the expected topology five days later. Average misalignment angles of 20°–40° have been reported for comparisons between observed loops and extrapolated potential field lines (Sandman et al. 2009). However, the comparison with the PFSS field lines and flare ribbon locations (see also Figure 5) is helpful to confirm that the combined 193 Å and 211 Å loop path corresponds more closely to the topology of the higher and longer blue field lines, whereas the 171 Å loop corresponds to the topology of the lower and shorter red field lines.

As a further check to investigate if the anti-phase transverse oscillations are a result of line of sight effects, we perturb the groups of field lines shown in Figure 4 assuming a horizontally polarized fundamental kink mode, and create space-time diagrams using the cuts shown in Figure 2 that are used to analyze the observational loop oscillations. To model the oscillations we perturb the field lines following the method of Verwichte et al. (2009). Figure 6 shows the displacement time curves of field lines determined from a cut (location shown in panel (a)) assuming either a horizontally or vertically polarized fundamental kink mode. Panels (b) and (c) show the displacement time profiles we would expect if the red and blue bundles of field
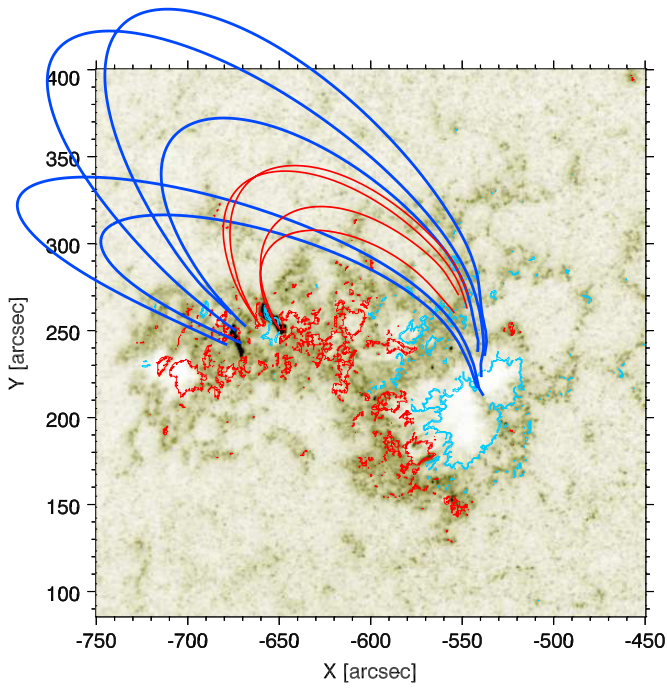
Figure 5. Field lines calculated using the PFSS model from 2012 May 13 are plotted on HMI line-of-sight magnetogram contours and an AIA 1600 Å reverse color image showing the positions of the flare ribbons. The HMI contours and AIA image are from 13:05 UT on 2012 May 8. Magnetic field contours are plotted at −300 and 300 G for the negative (blue contours) and positive (red contours) polarities, respectively.
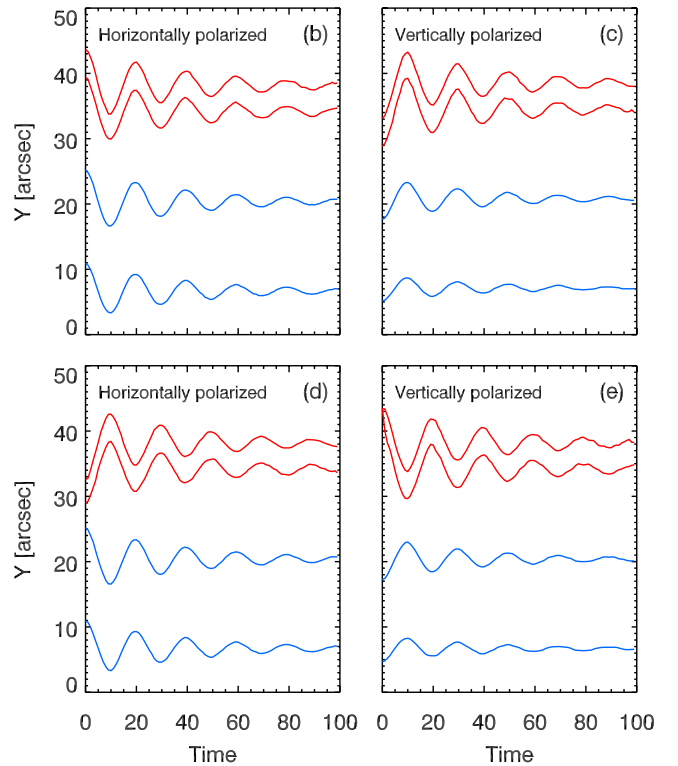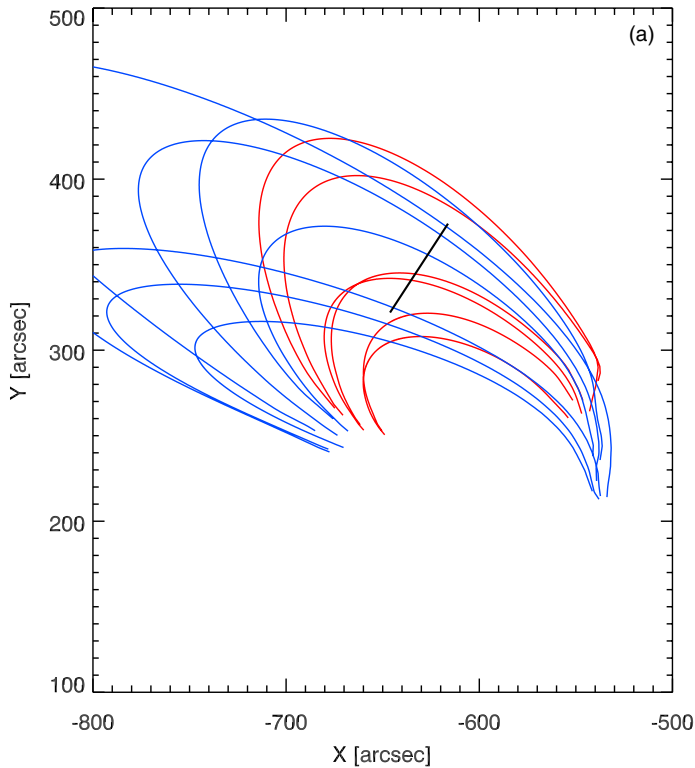
(A color version of this figure is available in the online journal.)

lines are oscillating in phase and panels (d) and (e) show the displacement time profiles we would expect if they are oscillating in anti-phase. This demonstrates that the observation of anti-phase TLOs is not a result of line of sight effects and that the loops themselves must be oscillating in anti-phase.

5. DISCUSSION

In this paper we have presented an *SDO*/AIA observation of a loop observed in the 171 Å bandpass that oscillates with a transverse motion in anti-phase with respect to loops observed in the 193 Å and 211 Å bandpasses. This observation of TLOs is unusual and counterintuitive when considering a flare blast wave excitation mechanism. A blast wave is often assumed to be the excitation mechanism for TLOs and should initially perturb the coronal loops away from the flare site.

The event occurs in the northern hemisphere and from the comparison between the AIA and *STEREO* fields of view, the loops are observed to be highly inclined together above the line of sight. This suggests that line of sight effects do not explain the anti-phase oscillations. Furthermore, the active region magnetic field was investigated with the PFSS extrapolation technique and the resulting field lines were perturbed assuming that the TLOs were either horizontally or vertically polarized. The PFSS extrapolation method gives an adequate first approximation of the local magnetic topology of an active region, however a truer picture of the topology can be obtained using force free models (Seehafer 1978, 1982; Wiegelmann 2008), which require vector rather than line-of-sight magnetic
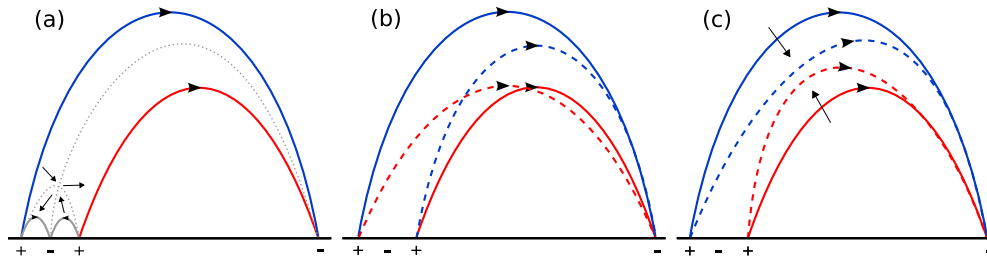

Figure 6. Figure demonstrating that the anti-phase transverse loop oscillations are not a result of line of sight effects but that field lines must be oscillating in anti-phase in order to produce an anti-phase signature. (a) The field lines obtained from the PFSS model. The red and blue groups of field lines are perturbed so that they oscillate either in phase or in anti-phase with each other. The black line indicates the cut taken to obtain space-time diagrams and is identical to the second from left cut in Figure 2. (b)–(e) Displacement time curves are shown for four field lines observed in the space-time diagrams for different polarizations of the kink mode and for the blue and red bundles of field lines oscillating either in phase or in anti-phase with one another. (b) Horizontally polarized kink mode, in phase perturbation. (c) Vertically polarized kink mode, in phase perturbation. (d) Horizontally polarized kink mode, anti-phase perturbation. (e) Vertically polarized kink mode, anti-phase perturbation.

(A color version of this figure is available in the online journal.)

Figure 7. (a) Sketch showing the direction of the velocity field indicated by the arrows assuming a 2D reconnection process. (b) Example of how slipping field lines reconfigure from the initial plain field lines into the dashed field lines. (c) The arrows show the initial anti-phase direction of motion that adjacent loops might take if field lines are assumed to undergo slippage during the reconnection process.

(A color version of this figure is available in the online journal.)

field data. In this study the PFSS model is sufficient as a first investigation into how an observation of anti-phase TLOs links with the local magnetic topology, but future studies should take this into account. From this analysis we rule out the possibility that the anti-phase oscillations are a result of an outside flare blast wave. Here the inwardly directed anti-phase nature of these oscillations suggests that the excitation is a local effect that is linked with the local magnetic topology of the region.

A previously reported example of anti-phase TLOs was presented by Schrijver & Brown (2000). Here they linked the behavior of the oscillations with the local magnetic topology of the region and the perturbation of null points. They suggest that a photospheric disturbance such as a sunquake may perturb the null points and so excite oscillations. In our observation, however, we do not see any signatures of photospheric disturbances. Anti-phase behavior has also been observed in Doppler shift observations with SUMER (Kliem et al. 2002) between hot (10^7 K) and cooler (2×10^4 K) plasma. In the SUMER observation they rule out TLOs as the reason behind the anti-phase signatures because the oscillation amplitudes are large compared with the height of the observations. There are, however, some similarities of the SUMER observations with this work where oscillations in the cooler bandpass (171 Å) are in anti-phase with respect to the oscillations seen in the slightly hotter bandpasses (193 Å and 211 Å).

The impulsive nature and the inwardly directed anti-phase motion of the observed TLOs suggests that the excitation could be linked to the flare reconnection process. Longcope & Tarr (2012) studied reconnection at a current sheet by modeling a two-dimensional (2D) quadrupolar field and analyzing the energy conversion to fast magneto-acoustic waves. They study the dynamics of the external field and show that the velocity field above and below the current sheet is directed inward (illustrated in their Figure 4). Our observations of anti-phase TLOs might then be explained as the signature of reconnection occurring in this active region. Figure 7(a) is a simplified model of the observed loops (solid lines) with the direction of the velocity field assuming a 2D reconnection model indicated by the arrows. In this case we would not expect anti-phase motion of the two loops because the velocity fields are directed in approximately the same direction. If this mechanism were to excite anti-phase oscillations, then the loops must have their western (and eastern) foot points in opposite polarities to one another. A further limitation of this model is that it is in 2D and studies have shown that reconnection in 3D can be significantly different (Pontin 2011).

Panels (b) and (c) of Figure 7 illustrate the idea of slipping field lines. The slipping of field lines may occur either as a result of reconnection involving a 3D null point or slip-running

reconnection. Figure 7(b) illustrates how field lines can change their connectivities through field line slippage. One of the foot points is held fixed (the negative polarity on the right hand side in this case) and the left hand foot points anchored in one positive polarity are allowed to slip over to the other positive source, so that the initial solid field lines end as the dashed field lines. In this observation we do not directly observe the slipping of field lines and we find that the oscillating loops end up at similar locations to where they started from. Figure 7(c) shows how field lines not directly involved in the reconnection process might then be perturbed by the slipping field lines. It provides an explanation of how inwardly directed TLOs may be excited in this observation.

3D reconnection at isolated null points has been split into three regimes: torsional spine, torsional fan, and spine-fan reconnection (Priest & Pontin 2009). Reconnection has also been proposed to occur in systems with multiple null points connected by separators, called separator reconnection (Pontin & Craig 2006), where current layers may form along the separator lines. For the torsional spine (fan) regime, a rotational perturbation of the fan plane (around the spine) causes current layers to build up in a tube around the spine (in the fan plane). In both cases the reconnection takes the form of rotational slippage of field lines which is dependent on the direction of the current with respect to the spine or the fan plane. It is expected that the most common form of reconnection to occur at 3D null points is spine-fan reconnection (Pontin 2011). Here a shear perturbation of either the spine or the fan causes the null point to collapse (the spine and fan collapse toward each other) and a current sheet forms across both the spine and fan. In our observations it is possible that a 3D null point has collapsed and that spine-fan reconnection is occurring. The slightly inward motions prior to the oscillation excitation (Section 3) and the low altitude release of energy may be further evidence that a null point has collapsed as field lines (and so loop structures) are initially drawn inward toward the null point.

A two stage reconnection model with a fan-spine configuration was proposed by Török et al. (2009) motivated by *Hinode/XRT* observations of an event on the solar limb next to a quiet prominence cavity. During the first reconnection stage in their 3D numerical simulations, one can see field lines on either side of the emerging flux show apparent motions toward the null point. Torsional Alfvén waves are also driven by the reconnection and are observed to propagate along the arcade field lines; the apparent inward motion of some of the field lines as a result of the torsional wave might again explain the inwardly directed anti-phase loop oscillations we observe. However, we need to be careful when comparing field line oscillations with oscillations of coronal structures since these Alfvén waves are

perturbations of individual field lines, whereas the transverse oscillations of density enhanced loops are interpreted as kink waves. Moreover, we note that the simulation by Török et al. (2009) includes a prominence flux rope that is not present in our event. This introduces effects such as extra twist, which may effect the perturbation of the field lines observed in the simulation.

3D non-null point reconnection models built on the concept of quasi-separatrix layers (QSLs), e.g., magnetic surfaces where there are strong gradients in the field line mapping (Demoulin et al. 1996) have been developed. QSLs are regions of enhanced current where magnetic reconnection is triggered if the current layers formed along QSLs are thin and dense enough (Demoulin et al. 1996). An example of a similar active region to the one we studied is shown in Demoulin et al. (1997, Figure 5(d)). Here the QSLs have been plotted along with typical field lines on either side of the QSLs. Instead of the 2D picture of reconnection about an X point where field lines change topological connections, 3D field lines might instead undergo slip-running reconnection (Aulanier et al. 2006) where the field lines slip along one another and across the QSL boundary. If slip-running reconnection is the excitation mechanism behind the oscillations then we might expect the larger loop to shrink, the smaller loop to grow, or a combination of the two. Figure 3 shows that the loops are initially about 10 Mm from one another in the cuts but at the end of the impulsive oscillations they are located at the same line-of-sight position at the location of the cut. This suggests that the loops have been pulled together and perhaps even merged during the observation. This is further evidence in support of a slip-running reconnection excitation mechanism. X-ray coronal loop slippage triggered by a flare has been observed by *Hinode*/XRT (Aulanier et al. 2007). That observation shows the loop foot points slipping over a duration of about 3.5 hr. Sometimes the loops show apparent motions in opposite directions, interpreted as a signature of the slip-running reconnection. Slip-running reconnection of field lines has also been observed to occur numerically before and after 3D null point reconnection in a region where a 3D null point is embedded within a QSL (Masson et al. 2009). Our observation of anti-phase loop oscillations may be a signature of field lines undergoing slip-running reconnection happening close to the EUV flare emission or in the vicinity of a 3D null point.

Another unusual feature of our observation is that the smaller 171 Å loop oscillates with an average period that is approximately 50 s longer than the loops observed in the 193 Å and 211 Å bandpasses. Although this slightly longer period is within 2σ of the 193 Å and 211 Å loop periods, it is seen in the cuts in Figure 3. Table 1 shows that the linear change in period for the 171 Å loop is 0.179, compared with 0.071 and 0.059 for the 193 Å and 211 Å loops, respectively. Increases in periods may be associated with growing loop lengths. Assuming that the transverse oscillations are fundamental kink modes, the phase speed, $V_{\rm ph} = 2L/P$, is lower for the smaller 171 Å loop compared to the larger 193 Å and 211 Å loops. A lower value of the phase speed indicates a lower value for the average magnetic field strength of the loop. From the PFSS model, the blue field lines are anchored in the sunspot region on the western side whereas the red field lines are anchored just above this region. We then expect the blue field lines to have a larger average magnetic field strength compared to the red field lines. This would cause the oscillation period of the red field lines to be slightly longer. Since the red field lines are an approximate match for the 171 Å loop and the 193 Å and 211 Å loops align better with the

blue field lines, this gives an explanation for the slightly longer period observed for the 171 Å loop.

We propose that in this observation the transverse oscillations are excited by the flare reconnection processes and in particular that they are the signatures of slipping field lines either as a direct result of slip-running reconnection or reconnection involving a 3D null point. Field lines shown in Figure 5 might slip across QSLs (or in the vicinity of a null point) situated close to the eastern loop foot points, which then perturb the thick blue field lines causing them to move downward and the thin red field lines to move out and upward. As a result the loops would move in anti-phase with respect to one another. This observation suggests that TLOs can be used as a tool to probe the local magnetic topology and can indicate, for example, where the slipping of field lines is taking place. Slipping field lines are difficult to observe in EUV observations but TLOs are comparatively easier to observe with instruments such as AIA. Observations such as this can then complement extrapolation techniques to build up a detailed picture of an active region magnetic topology and to study any dynamic processes such as the slipping of field lines due to reconnection that may be occurring.

REFERENCES

Asai, A., Ishii, T. T., Isobe, H., et al. 2012, ApJL, 745, L18
Aschwanden, M. J., de Pontieu, B., Schrijver, C. J., & Title, A. M. 2002, SoPh, 206, 99
Aschwanden, M. J., Fletcher, L., Schrijver, C. J., & Alexander, D. 1999, ApJ, 520, 880
Aschwanden, M. J., & Schrijver, C. J. 2011, ApJ, 736, 102
Aulanier, G., Golub, L., DeLuca, E. E., et al. 2007, Sci, 318, 1588
Aulanier, G., Pariat, E., Démoulin, P., & DeVore, C. R. 2006, SoPh, 238, 347
Boerner, P., Edwards, C., Lemen, J., et al. 2012, SoPh, 275, 41
De Moortel, I., Ireland, J., & Walsh, R. W. 2000, A&A, 355, L23
Demoulin, P., Bagala, L. G., Mandrini, C. H., Henoux, J. C., & Rovira, M. G. 1997, A&A, 325, 305
Demoulin, P., Henoux, J. C., Priest, E. R., & Mandrini, C. H. 1996, A&A, 308, 643
Foullon, C., Fletcher, L., Hannah, I. G., et al. 2010, ApJ, 719, 151
Gosain, S., & Foullon, C. 2012, ApJ, 761, 103
Hershaw, J., Foullon, C., Nakariakov, V. M., & Verwichte, E. 2011, A&A, 531, A53
Hori, K., Ichimoto, K., Sakurai, T., Sano, I., & Nishino, Y. 2005, ApJ, 618, 1001
Howard, R. A., Moses, J. D., Vourlidas, A., et al. 2008, SSRv, 136, 67
Kiddie, G., De Moortel, I., Del Zanna, G., McIntosh, S. W., & Whittaker, I. 2012, SoPh, 279, 427
Kliem, B., Dammasch, I. E., Curdt, W., & Wilhelm, K. 2002, ApJL, 568, L61
Krishna Prasad, S., Banerjee, D., & Singh, J. 2012a, SoPh, 281, 67
Krishna Prasad, S., Banerjee, D., Van Doorsselaere, T., & Singh, J. 2012b, A&A, 546, A50
Lemen, J. R., Title, A. M., Akin, D. J., et al. 2012, SoPh, 275, 17
Longcope, D. W., & Tarr, L. 2012, ApJ, 756, 192
Ma, S., Raymond, J. C., Golub, L., et al. 2011, ApJ, 738, 160

Markwardt, C. B. 2009, in ASP Conf. Ser. 411, Astronomical Data Analysis Software and Systems XVIII, ed. D. A. Bohlender, D. Durand, & P. Dowler (San Francisco, CA: ASP), 251

Masson, S., Pariat, E., Aulanier, G., & Schrijver, C. J. 2009, ApJ, 700, 559

McIntosh, S. W., de Pontieu, B., Carlsson, M., et al. 2011, Natur, 475, 477

Muhr, N., Veronig, A. M., Kienreich, I. W., Temmer, M., & Vršnak, B. 2011, ApJ, 739, 89

Nakariakov, V. M., & Ofman, L. 2001, A&A, 372, L53

Nakariakov, V. M., Ofman, L., Deluca, E. E., Roberts, B., & Davila, J. M. 1999, Sci, 285, 862

Nakariakov, V. M., & Verwichte, E. 2005, LRSP, 2, 3

Nisticò, G., Nakariakov, V. M., & Verwichte, E. 2013, A&A, 552, A57

Pontin, D. I. 2011, AdSpR, 47, 1508

Pontin, D. I., & Craig, I. J. D. 2006, ApJ, 642, 568

Priest, E. R., & Pontin, D. I. 2009, PhPl, 16, 122101

Roberts, B. 2000, SoPh, 193, 139

Sandman, A. W., Aschwanden, M. J., Derosa, M. L., Wülser, J. P., & Alexander, D. 2009, SoPh, 259, 1

Schatten, K. H., Wilcox, J. M., & Ness, N. F. 1969, SoPh, 6, 442

Schrijver, C. J. 2001, ApJ, 547, 475

Schrijver, C. J., Aschwanden, M. J., & Title, A. M. 2002, SoPh, 206, 69

Schrijver, C. J., & Brown, D. S. 2000, ApJL, 537, L69

Schrijver, C. J., & De Rosa, M. L. 2003, SoPh, 212, 165

Seehafer, N. 1978, SoPh, 58, 215

Seehafer, N. 1982, SoPh, 81, 69

Tomczyk, S., McIntosh, S. W., Keil, S. L., et al. 2007, Sci, 317, 1192

Török, T., Aulanier, G., Schmieder, B., Reeves, K. K., & Golub, L. 2009, ApJ, 704, 485

Tothova, D., Innes, D. E., & Stenborg, G. 2011, A&A, 528, L12

Van Doorsselaere, T., Birtill, D. C. C., & Evans, G. R. 2009, A&A, 508, 1485

Van Doorsselaere, T., Nakariakov, V. M., Young, P. R., & Verwichte, E. 2008, A&A, 487, L17

Verwichte, E., Aschwanden, M. J., Van Doorsselaere, T., Foullon, C., & Nakariakov, V. M. 2009, ApJ, 698, 397

Verwichte, E., Foullon, C., & Van Doorsselaere, T. 2010, ApJ, 717, 458

Verwichte, E., Nakariakov, V. M., Ofman, L., & Deluca, E. E. 2004, SoPh, 223, 77

Verwichte, E., Van Doorsselaere, T., Foullon, C., & White, R. S. 2013, ApJ, 767, 16

Wang, T., Ofman, L., Davila, J. M., & Su, Y. 2012, ApJL, 751, L27

Wang, T. J., Solanki, S. K., Curdt, W., et al. 2003, A&A, 406, 1105

White, R. S., & Verwichte, E. 2012, A&A, 537, A49

White, R. S., Verwichte, E., & Foullon, C. 2012, A&A, 545, A129

Wiegelmann, T. 2008, JGRA, 113, 3